Development of Dual-eyes Docking System for AUV with Lighting 3D Marker*

1st Sho Nakamura
Graduation school of Natural Science and Technology, Okayama University
Okayama, Japan
pc7y9wqz@s.okayama-u.ac.jp

2nd Daiki Yamada
Graduation school of Natural Science and Technology, Okayama University
Okayama, Japan
p7kw2h27@s.okayama-u.ac.jp

3rd Naoki Mukada
Graduation school of Natural Science and Technology, Okayama University
Okayama, Japan
pola9zud@s.okayama-u.ac.jp

4th Myo Myint
Thanlyin Technological University
Yangon, Myanmar
puqs1ci8@s.okayama-u.ac.jp

5th Khin New Lwin
Graduation school of Natural Science and Technology, Okayama University
Okayama, Japan
pdoj8yez@s.okayama-u.ac.jp

6th Takayuki Matsuno
Graduation school of Natural Science and Technology, Okayama University
Okayama, Japan
matsuno@cc.okayama-u.ac.jp

7th Yuichiro Toda
Graduation school of Natural Science and Technology, Okayama University
Okayama, Japan
ytoda@s.okayama-u.ac.jp

8th Mamoru Minami
Graduation school of Natural Science and Technology, Okayama University
Okayama, Japan
minami-m@cc.okayama-u.ac.jp

***Abstract*—This paper presents that our proposed docking system could apply for a new Remotely Operated Vehicle(ROV). The authors have proposed a 3D-perception based Move on Sensing (3D-MoS) system using a new 3D position and orientation (pose) estimation method with dual-eye camera that exploits the parallactic nature that enables reliable 3D pose estimation in real-time, named as "Real-time Multi-step Genetic Algorithm (RM-GA)." We confirmed ROV have conducted docking that assumes charging battery under water by the system, having shown it effective. As a next step, docking experiment using the new ROV were conducted to verify the proposed system apply for new ROV. But, the new ROV is different from a ROV that have used previous experiments, on the point of thruster setting structure. Then, a new control system using Jacobian that shows relationship voltage and velocity was constructed. After it is confirmed the system is effective, docking experiments in the pool have been conducted. In this report, the structure and result of experiments are reported in detail.**

***Index Terms*—Autonomous Underwater Vehicle, Dual-eye Camera, Visual Servoing**

I. Introduction

Nowadays, docking operation is standing as a critical challenge for autonomous underwater vehicles with such applications as sleeping under mother ship, recharging batteries, transferring data and new mission uploading. Research on the docking system using various homing sensors [1]- [3] and techniques [4]- [6] for the underwater robot has been conducted worldwide. Even though expensive navigation sensor suit and large scale dead reckoning sensors are able to provide accurate position data, the final approach of docking process especially for unidirectional docking station is still a difficult task. To achieve this task, visual-based docking system have been reported with the rapid progresses in computer vision technology recently. Some works are based on one camera [7]- [10] and implemented using two cameras. Even though two cameras are used in [11] [12]. Visual servoing using 3D maker and dual-eye camera that means seeing the same object at the same time by both two cameras has not been applied. In general, one camera is used for pose estimation and the other for another tasks. In contract, we have developed visual-based docking system for underwater vehicle using stereo vision. To the best knowledge of author, our proposed system is the first initiated research using stereo vision in underwater vehicle environment. What we have confirmed in [13] is that the docking process using proposed system has high homing accuracy.

Even though the robustness of the proposed system against different kinds of disturbances and the effect of the illumination variation under arbitrary light condition were confirmed in previous work [14] and [15], the versatility of proposed system have not been confirmed. Then, to verify the versatility of proposed system, docking experiments for new ROV were conducted.

Figure 1 shows a photo of KOWA ROV. Figure 2 shows overview of KOWA ROV. It was used as a test bed. In [16], docking experiments using stereo vision was achieved and proved the effectiveness of the proposed system for KOWA ROV. However the used ROV's thrusters construction is orthogonal. The ROV has less cruise ability but easy for controlling. Therefore, docking experiments using other

978-1-5386-4814-8/18/$31.00 ©2018 IEEE

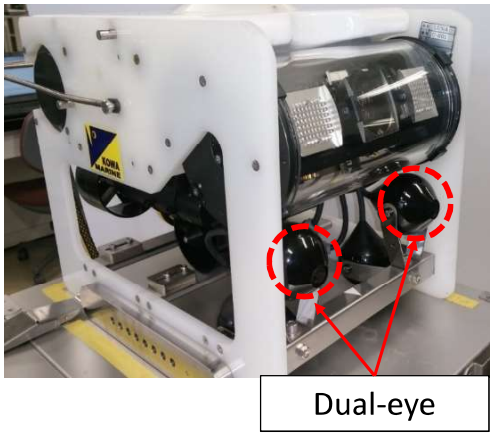

Fig. 1. Remotely Operated Vehicle (KOWA ROV)

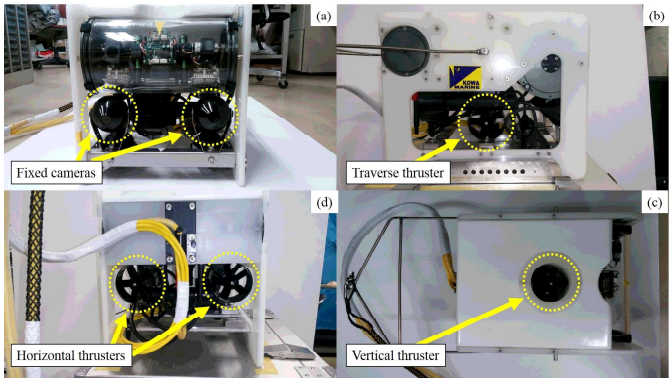

Fig. 2. Overview of KOWA ROV (a)Front View (b)Side View (c)Top View (d)Back View

ROV have been conducted to verify the versatility of our system. Then, a new ROV(QI ROV) that is manufactured by Quality and Innovation corporation is used for docking experiments. Figure 3 shows a photo of QI ROV. Figure 4 shows configuration of thrusters for QI ROV. Configuration of thruster of two vehicles is different. Because QI ROV has V-shaped thruster, there are some complex coupling between each thruster.

In this study, we have developed QI ROV and conducted docking experiments in the pool to assess the system performance. Since the configuration of thrusters in the new ROV is not simple same as the one used in previous experiments, it was improved the control system considering the dynamic coupling between each other. In the control method, coupling of thrusters to each other were checked, and inverse Jacobian matrix was optimized experimentally. After adjusting parameters, the docking performance under day and night environment was verified by conducting docking experiment in the pool.

This paper is organized as follows:Section II presents the proposed docking system for ROV. Section III describes control system construction experiment. Section IV describes check experiment of a control system. Section V describes the docking experiments in the pool. The final section contains the conclusions of this study.

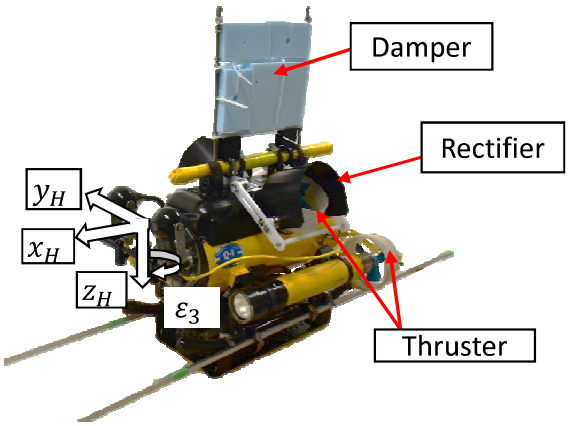

Fig. 3. QI ROV(DELTA-150)

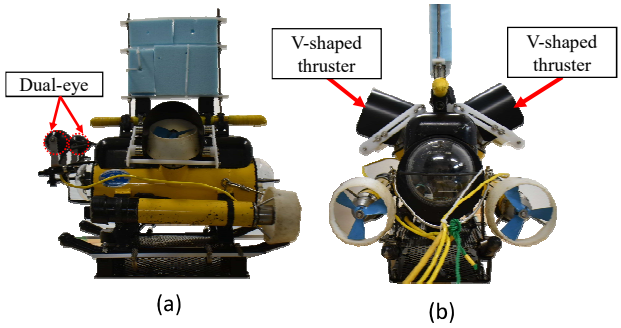

Fig. 4. Configuration of thruster for QI ROV (a)Side View (b)Back View

II. PROPOSED DOCKING SYSTEM

A. Docking Strategy

In an underwater battery recharging operation, the Autonomous Underwater Vehicle(AUV) must navigate to a seafloor station and dock at the station for recharging. Normally, a cone-shaped docking station with light sources mounted around its entrance is used for a torpedo-shaped AUV. The hovering-type AUV studied in [17] docks by descending to the station. To perform docking experiments for underwater automatic charging using the proposed approach, a rod was installed on the right side of the underwater robot, and a matching cylindrical hole was attached to the left side of the target. When the ROV is in the correct pose relative to the

object, it must move forward to insert the rod into the hole. A flowchart of the proposed docking method is shown in Fig. 5. This method is divided into the five steps: (a) approaching, (b)visual servoing, (c)docking, (d)docking completion, and (e)stay and data storing. In the approaching step, the AUV estimates its approximate position relative to the station using other methods, such as an acoustic method, and approaches the station. The approaching step was performed manually in this study. In the visual servoing step, the AUV measures the precise relative pose using stereo-vision-based estimation and remains at the entry point for the final docking step, as shown in Fig. 6(a).

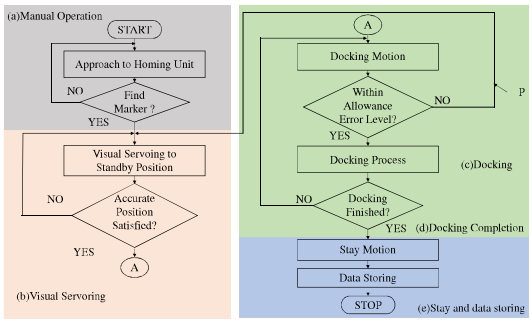

Fig. 5. Docking operation steps, including approaching, visual servoing, and docking. Note that approaching is performed by manual control at the beginning of the docking operation in this study. The error allowance for docking is ± 50 mm in the y- and z-directions and $\pm 7^{\circ}$ in the rotation about the z-axis.

In the docking step, the AUV moves to the final desired pose, as shown in Fig. 6(b) as long as the errors of the y- and z-components of the position of the ROV and that of its orientation about the z-axis relative to the target remain within ± 50 mm and $\pm 7^{\circ}$, respectively, for a minimum of 165 ms (five times the length of the control loop). Whenever any of these components of the error of the relative pose exceeds this allowance, the process switches to visual servoing, as shown by the path labeled "P" in Fig. 5. This process of switching between the visual servoing and docking steps was implemented to avoid any physical damage that could result from contact between the rod and the hole in the target. In the completion of docking step, the ROV keeps the desired pose especially at the 350 mm distance in x-axis direct to store the experimental data from memory to hard-disk of PC. This process is named as stay in this docking strategy. After storing the experiment data, the vehicle moves back to 600 mm distance in x-direction for next docking operation.

B. Model-based Matching using Multi-Step GA

Apart from other recognition methods based on 2D to 3D reconstruction, the proposed 3D model-based recognition is based on 3D to 2D projection. Moreover, the concept based on the group of pixels rather than individual pixels highlights merits of model-based method over feature-based ones. Pose of target object is estimated using model-based matching based on known 3D model of the target projected to 2D images. Target object is the 3D marker that consists

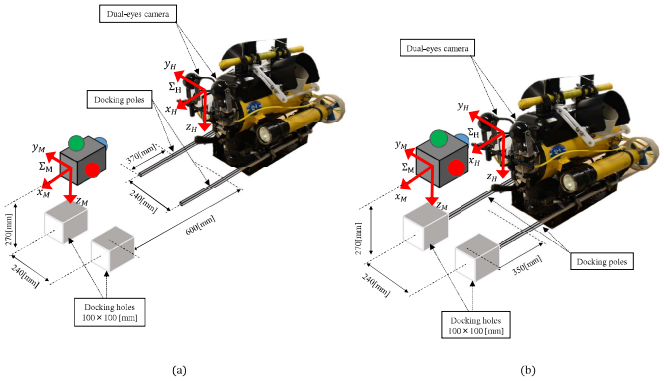

Fig. 6. Layout of the docking experiment showing the process of aligning the ROV with the 3D marker. (a) Desired pose in the visual servoing step. (b) Desired pose at the completion of the docking step. Σ_M and Σ_H denote the coordinate systems of the 3D marker and the ROV, respectively. The pose of the marker relative to the ROV, represented by the position and orientation of Σ_M with respect to Σ_H, is considered to be the unknown in the 3D pose estimation process.

of three spheres (40[mm] in diameter) whose colors are red, green and blue. Knowing the information of the target and predefined relative pose to the ROV, the solid model of the target is predefined and projected to 2D images. Comparing the projected solid model image with the captured 2D images by dual cameras, the relative pose difference is calculated. We have confirmed the pose that have the highest fitness function value represents the pose of the real target. Therefore the problem of pose recognition addresses to the searching problem. The solution is GA with promising speed and accuracy of performance. According to the performance in time-domain, GA is selected in this work even though there are advanced optimized techniques. The effectiveness of 1-step GA was confirmed in robots especially manipulators and reported in previous work [18]- [23]. The stability of the system was also confirmed by means of Lyapunouv analysis in previous work[21]. Through the steps of GA (Selection, Cross over and Mutation), a number of genes that represent different poses are evaluated by the defined fitness function to get the best gene with the most truthful estimated pose. A correction function representing a matching degree of projected model against the real target in the image, which is a correction function of real target projected in camera images with the assumed model represented by poses in genes, is used as a fitness function in GA process. The convergence of GA is realized in the sequences of dynamic images input by video rate [30 frames/s]. Detail discussion about 1-Step GA and fitness function are explained in [19]. The number of evolving generations in this experiment is 9 per 33 [ms] and the number of genes is 60.

C. Fitness Function

The fitness function is constructed to evaluate the matching degree between the projected model and the captured image. The optimum searching and the GA convergence speed were effected by the construction of the fitness function. The

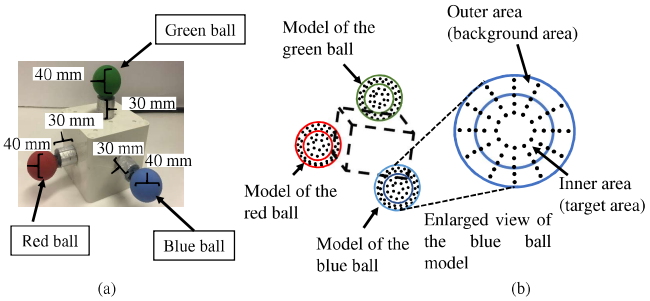

Fig. 7. Real 3D marker and model: (a) active/lighting marker, (b) model with enlarged view of the blue ball model, where the inner area is the same size as the real target object (blue ball) and the outer area is the background area. The dots in enlarged view of blue ball mean points to calculate the correlation degree on how much the inner area overlaps the blue ball and the outer area does not overlap the blue ball.

calculation of fitness value of each individual model can be done repeatedly in genetic algorithm. Figure 7 shows the real target and model of 3D marker. Hue value and brightness value is used for recognition of 3D marker because of less sensitive to the environment. Each model consists of three spherical ball (red, green and blue). Each spherical ball consists of two portions, where the inner portion is the same size as the real target object and the outer area is the background area. The dots in each ball mean points to calculate the correlation degree on how much the inner area overlaps the target object and the outer area does not overlap the target object. The captured image (pixel) is detected in 2D image as (green or blue or red) in hue space. If the captured image (pixel) situated in inner portion, the fitness value will be increased and the capture image (pixel) is situated in outer portion, the fitness value will be decreased. Therefore, the fitness value will be maximum when the model and the real target are identical. Finally, the pose of the model with the maximum fitness value is thought to represent the pose of the real target 3D marker. Position and orientation information is output in a three-dimensional. Detailed explanation about the fitness function is referred to our previous paper [24].

D. Active/Lighting Maker

In previous experiment, the passive marker was used to conduct the 3D pose estimation and the docking performance. In the present study, the active marker was designed and constructed to improve the pose estimation at high turbidity level in day and night time. Figure 8 shows the appearance of the active/lighting marker. The circuit was created by combining the variable resistors, resistors, and the light emitting diodes such as red, green, and blue. The resistance value of the variable resistors, and the number of resistors are determined by trial and error. The 3D marker is constructed from a water proof box (100 mm $\times$ 100 mm $\times$ 100 mm) and the white spheres (diameter: 40 mm) are attached to the water proof box. The red, green and blue LED were installed into the white spherical ball and covered by the color balloon as shown in Fig. 8. The 3D pose estimation can be improved by emitting the light of LED from 3D marker under day and night environment.

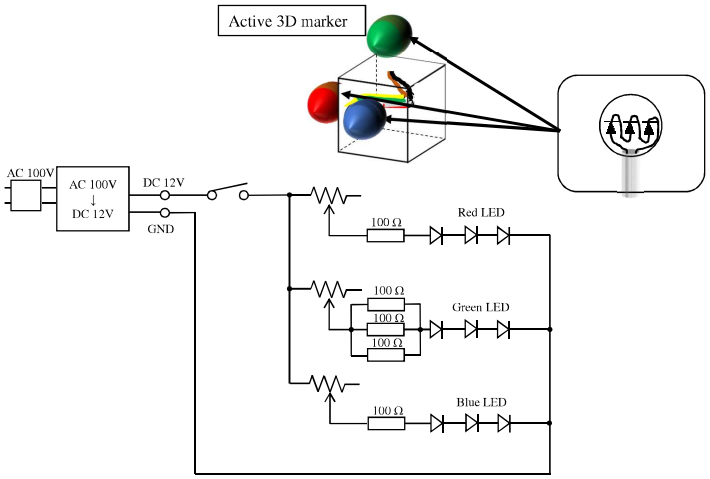

Fig. 8. Active/Lighting 3D marker: Red, green and blue LED were installed into the white spherical ball and covered by colour balloon. The resistance value of the variable resistors, and the number of resistors are determined by trial and error.

III. Proportional Controller with Inverse Jacobian

The block diagram describing the control system is shown in Fig. 9. The four thrusters mounted on the ROV are controlled by sending the command voltage ($\mathbf{v} = (v_x, v_y, v_z, v_{\epsilon 3})$) based on the feedback relative pose between the current estimated pose ($\hat{x}$, $\hat{y}$, $\hat{z}$, $\hat{\epsilon_3}$) of the ROV represented by Σ_H in Fig. 3 and the desired pose (x_d, y_d, z_d, ϵ_{3d}).

In the present study, the control of rotation around the x-axis and y-axis in Σ_H was neglected because the structure of the underwater robot (center of buoyancy to be located above the center of gravity) is autonomously restored to a stable horizontal state. Since there is coupling effect among thrusters, it is modified the controller with consideration of relation among thrusters. Therefore, we added inverse of Jacobian, $\mathbf{J^{-1}}$ in the controller. Inverse Jacobian matrix (4 $\times$ 4) was experimentally calculated as follows:

Equation (1) shows the relation between the speed of the vehicle and input voltage through Jacobian matrix.

$$\begin{bmatrix} \dot{x}^{(1)} & \cdots & \dot{x}^{(n)} \\ \dot{y}^{(1)} & \cdots & \dot{y}^{(n)} \\ \dot{z}^{(1)} & \cdots & \dot{z}^{(n)} \\ \dot{\varepsilon}_3^{(1)} & \cdots & \dot{\varepsilon}_3^{(n)} \end{bmatrix} = \begin{bmatrix} J_{11} & J_{12} & J_{13} & J_{14} \\ J_{21} & \cdot & \cdot & \cdot \\ J_{31} & \cdot & \cdot & \cdot \\ J_{41} & \cdot & \cdot & \cdot \end{bmatrix} \begin{bmatrix} {v_x}^{(1)} & \cdots & {v_x}^{(n)} \\ {v_y}^{(1)} & \cdots & {v_y}^{(n)} \\ {v_z}^{(1)} & \cdots & {v_z}^{(n)} \\ {v_{\varepsilon 3}}^{(1)} & \cdots & {v_{\varepsilon 3}}^{(n)} \end{bmatrix} \quad (1)$$

$$\mathbf{Q} = \mathbf{JP} \quad (2)$$

Here, the suffix (1 to n) at the upper right of the elements in the matrix indicates the number of speed observation trials. In order to obtain Jacobian matrix from observed velocity matrix

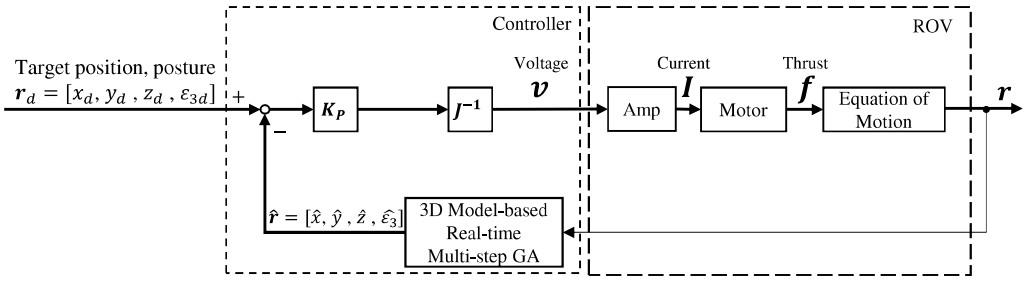

Fig. 9. Visual servoing system using feedback control

and voltage input matrix, pseudo inverse matrix is used. Let define the observation speed matrix as $\mathbf{Q}$ (matrix in the left side of Eq. (1)), the Jacobian matrix as $\mathbf{J}$ (left matrix in right side of Eq.(1)), the voltage input matrix as $\mathbf{P}$ (right matrix in right side of Eq. (1)). Eq.(2)) shows Relationship between the $\mathbf{Q}$ and $\mathbf{JP}$. The pseudo inverse matrix $\mathbf{P}^+$ of the voltage input matrix $\mathbf{P}$ can be obtained as follows:

$$\mathbf{P}^+ = \mathbf{P}^\mathbf{T} \left(\mathbf{P}\mathbf{P}^\mathbf{T}\right)^{-1} \tag{3}$$

Using Eqs. (2) and (3),

$$\begin{aligned} \mathbf{Q}\mathbf{P}^+ &= \mathbf{J}\mathbf{P}\mathbf{P}^+ \\ &= \mathbf{J}\mathbf{P}\mathbf{P}^\mathbf{T} \left(\mathbf{P}\mathbf{P}^\mathbf{T}\right)^{-1} \\ &= \mathbf{J} \\ \therefore \mathbf{J} &= \mathbf{Q}\mathbf{P}^\mathbf{T} \left(\mathbf{P}\mathbf{P}^\mathbf{T}\right)^{-1} \end{aligned} \tag{4}$$

$$\mathbf{J} = \begin{bmatrix} 0.050038 & -0.001523 & 0.000697 & -0.000021 \\ -9.216522 & 708.465722 & -0.246923 & -0.033058 \\ 2.061116 & 22.106510 & 86.981461 & -0.000266 \\ -1.592627 & -2.953606 & -9.903108 & 227.273366 \end{bmatrix} \tag{5}$$

Please note that the Jacobian matrix as shown in Eq .(5) was derived experimentally. The Jacobian matrix $\mathbf{J}$ can be expressed using the observation speed matrix with $\mathbf{Q}$ and the voltage input matrix $\mathbf{P}$. Therefore, the relation between the speed of QI ROV and the input voltage is given by the expression Eq .(6).

$$\begin{bmatrix} \dot{x} \\ \dot{y} \\ \dot{z} \\ \dot{\varepsilon}_3 \end{bmatrix} = \mathbf{J} \begin{bmatrix} v_x \\ v_y \\ v_z \\ v_{\varepsilon 3} \end{bmatrix} \tag{6}$$

The control voltages of the four thrusters are calculated as follows:

$$\begin{bmatrix} v_x \\ v_y \\ v_z \\ v_{\epsilon_3} \end{bmatrix} = \mathbf{J}^{-1}\mathbf{K_P} \begin{bmatrix} x_d - \hat{x} \\ y_d - \hat{y} \\ z_d - \hat{z} \\ \varepsilon_{3d} - \widehat{\varepsilon_3} \end{bmatrix} \tag{7}$$

In Eq. (7), v_{ϵ_3}, v_x, and v_y, and v_z are the control voltages of the four thrusters for the orientation around z-axis and movement of the ROV in the x, y, and z direction respectively. Here, x_d, y_d, z_d, and ϵ_{3d} specify the desired relative pose between the vehicle and the target. A proportional controller is used for all thrusters to control the vehicle in the docking experiment after confirming that the P controller is sufficient for this experiment. The gain coefficients $\mathbf{K_P}$=diag(K_{Px}, K_{Py}, K_{Pz}, $K_{P\varepsilon 3}$) are adjusted in order to achieve the best condition for visual servoing in the docking process based on preliminary experimental results.

IV. Check Experiment of a Control System

A. Constant position and orientation control experiment

Constant position and orientation control experiments were conducted by using QI ROV in the pool (length 2870 [mm] × width 2000 [mm] × height 1000 [mm]) filled with 4000 l of clear water. The physical disturbances were given from x,y,z-axis and rotation around z-axis. 30 s after the experiment was started, disturbances were given.

Desired positions are [x_d, y_d, z_d]=[600, 0, 0][mm], orientations that are represented in quaternion are ε_d=[ε_{d1}, ε_{d2}, ε_{d3}]=[0, 0, 0].

ε_1 and ε_2 that are represented the x_H and y_H axis of the orientation are keeping (0,0) for relationship between the buoyancy and the center of gravity. In this case, the allowable error range for each positions (x, y, z) is ± 50 [mm] and orientation around the z-axis is within 0.046 in quaternion.

Figure 11 shows an experimental result when the physical disturbance was given from y-axis. Recognition position and fitness value change in 30 s by disturbance. After disturbance was given, it has restored to the desired position and orientation. Since experimental results when the physical disturbances were given from x, z-axis and rotation around z-axis show same results, the robustness against physical disturbance can be verified. In this way, the effectiveness of our proposed control system is verified.

V. Docking Experiments in the Pool

A. Docking experiments in the pool in daytime

Docking experiment in a pool were conducted. The unidirectional docking station was designed as shown in Fig. 10. The station has two rectangle docking holes (100 [mm] × 100 [mm]) and a 3D active marker.

In this experiment, the two docking poles were attached to the left and right sides of the ROV for staying in front of

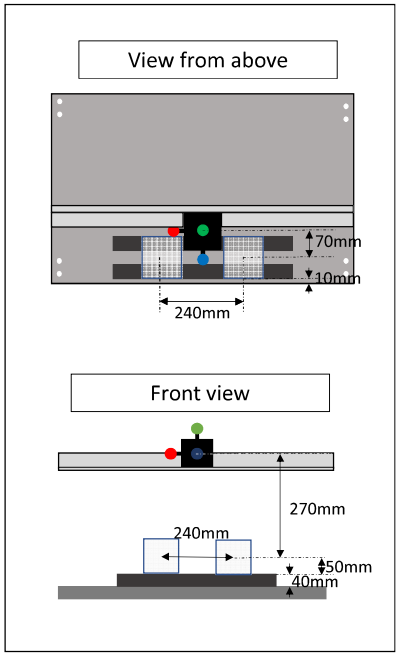

Fig. 10. Docking station

the docking station when the data was storing. The ROV is supposed to recharge during the staying process intended for battery recharging operation. Docking in the pool in day time is explained in detail in this section. The turbidity level was 0 FTU when the docking experiment was conducted. The fitness value of docking was above 0.8 as shown in Fig. 12(1-a).

The desired pose (x_d= 600 mm, y_d= 0 mm, z_d= 0 mm, ϵ_{3d}= 0 deg) between the ROV. When the ROV is stable in the above desired pose relative to the 3D marker, the ROV moves forward in order to insert the docking pole into the docking hole. In this case, the allowable error range for positions y, z is $\pm$ 40 [mm] and orientation around the z-axis is within 0.046 in quaternion.

Docking experiment results in the pool in day time are shown in Fig. 12(1-b),(1-c),(1-d),(1-e). The period from 150 s to about 160 s is the visual servoing step. After the ROV is stable in the allowance error ranges, the ROV moved forward to finish docking operation.

During the docking process, the ROV started inserting the docking pole into the docking hole by decreasing the distance from 600 mm to 350 mm. Finally, the docking step was completed at the time of 190 s from the start of the experiment. After about 190 s, the stay step was performed and the final log data were stored in files from memory into the hard disk. At that time, the ROV was controlled by giving the constant voltage to the forward thruster in x-axis direction.

B. Docking experiments in the pool in nighttime

Apart from daytime experiment as explained in previous section, the performance of the docking experiment in night-time is presented in this section. The turbidity level was 0 FTU when the docking experiment was conducted. The fitness value of docking was always above 0.8 as shown in Fig. 12(2-a). In this case, the allowable error range for positions is the same as daytime docking experiment. Pool docking experiment results in daytime are shown in Fig. 12(2-b),(2-c),(2-d),(2-e). The visual servoing started about 620 s. After starting the visual servoing step, the position along y-axis exceeds the error allowance range at the 640 s. However, the position along the y- and z-axes and orientation around z-axis are kept within the error allowance range by visual servoing until the end of the docking operation. The docking operation was performed between the about 640 s to 660 s and docking was completed after about 670 s.

VI. Conclusion

In this work, QI ROV was developed for docking experiments. Since the configuration of thrusters of ROV has coupling effects of thrust to each other, the motion controller was developed with inverse Jacobian. Constant position and orientation control experiment were conducted in the pool to verify the motion controller was developed. Finally, pool docking experiments were conducted. The experimental results showed the versatility of proposed system and verified to conducted docking experiments in day and night-time successfully.

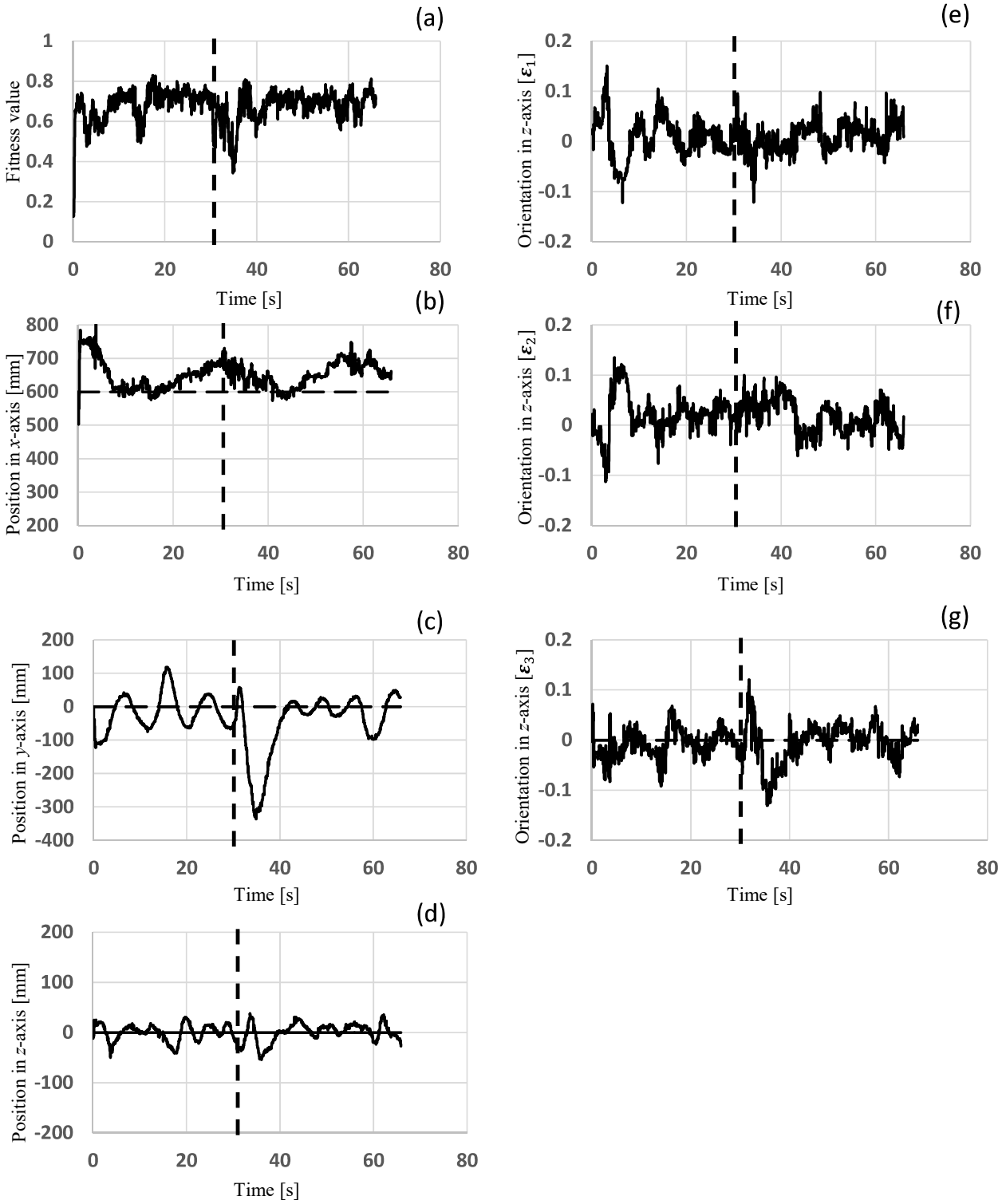

Fig. 11. Visual servoing results to constant position and orientation:(a) Fitness value, (b) Position in x-axis, (c) Position in y-axis, (d) Position in z-axis, (e) Rotation in x-axis, (f) Rotation in y-axis, (g) Rotation in z-axis

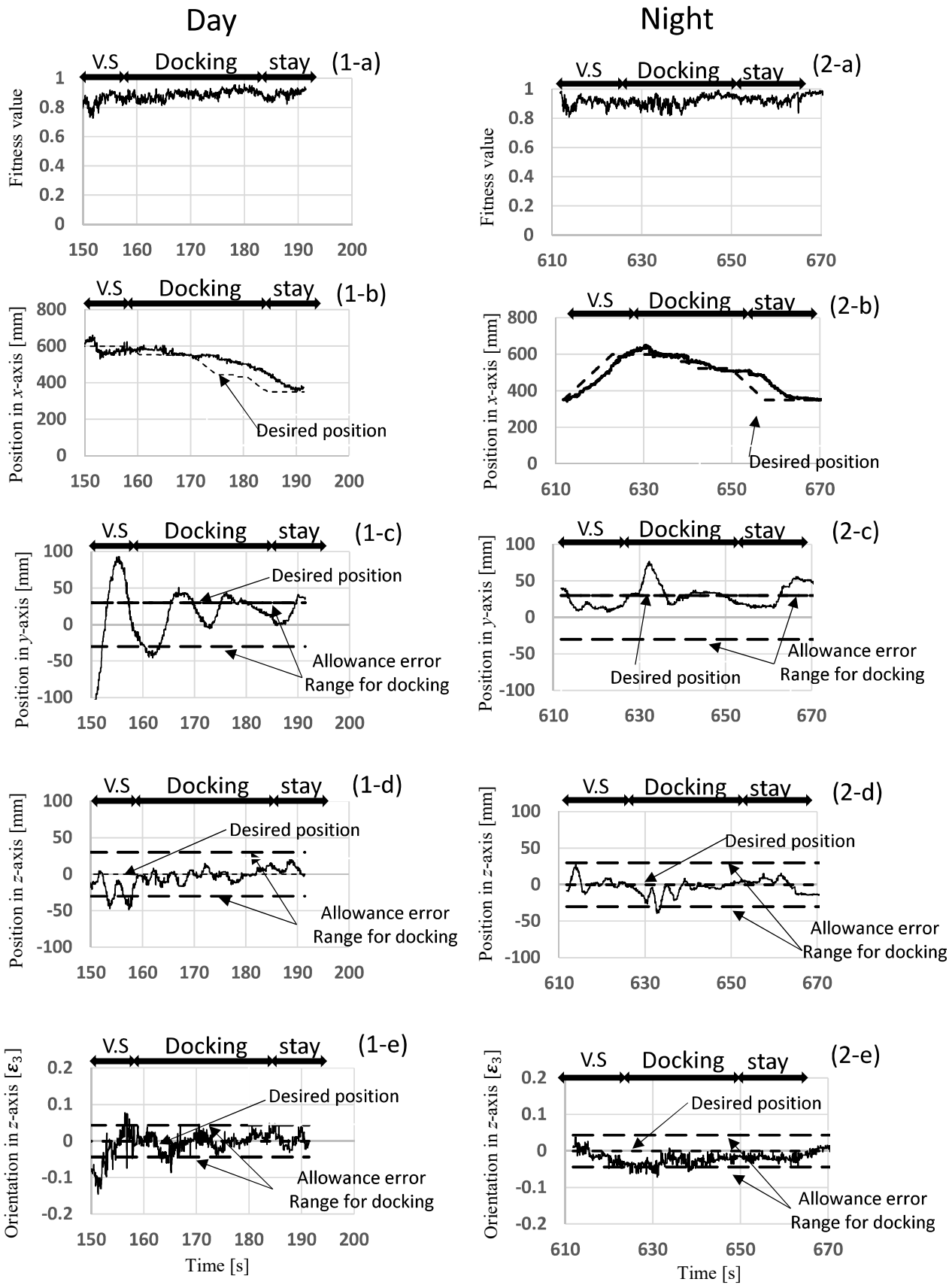

Fig. 12. Docking experiment result in a pool:(1-a) Fitness value in day time, (1-b) Position in x-axis in day time, (1-c) Position in y-axis in day time, (1-d) Position in z-axis in day time, (1-e) Rotation in x-axis in day time, (2-a) Fitness value in night time, (2-b) Position in x-axis in night time, (2-c) Position in y-axis in night time, (2-d) Position in z-axis in night time, (2-e) Rotation in x-axis in night time

VII. Acknowledgment

This work was supported by JSPS KAKENHI Grant Number 16K06183 and Mitsui E&S Holdings Co.,Ltd. and KOWA Co.,Ltd Marine System Department.

References

[1] Steve Cowen, Susan Briest and James Dombrowski, Underwater Docking of Autonomous Undersea Vehicle using Optical Terminal Guidance, Proc. IEEE Oceans Engineering, Vol.2, pp.1143-1147, 1997.

[2] Michael D. Feezor, F. Yates Sorrell, Paul R. Blankinship and James G. Bellingham, Autonomous Underwater Vehicle Homing/Docking via Electromagnetic Guidance, IEEE Journal of Oceans Engineering, Vol. 26, NO. 4, pp.515-521, October 2001.

[3] Robert S. McEwen, Brett W. Hobson, Lance McBride and James G. Bellingham, Docking Control System for a 54-cm-Diameter (21-in) AUV, IEEE Journal of Oceanic Engineering, Vol. 33, NO. 4,pp. 550-562, October 2008 .

[4] Ken Teo, Benjamin Goh and Oh Kwee Chai, Fuzzy Docking Guidance Using Augmented Navigation System on an AUV, IEEE Journal of Oceans Engineering, Vol. 37, NO. 2, April 2015.

[5] Ken Teo, E. An and P.-P. J. Beaujean, A robust fuzzy autonomous underwater vehicle (AUV) docking approach for unknown current disturbances, IEEE Journal of Oceanic Engineering, Vol. 37, No. 2, pp.143-155, April 2012.

[6] Amaury N' egre, C edric Pradalier and Matthew Dunbabin, Robust vision-based underwater homing using self similar landmarks, Journal of Field Robotics, Wiley-Blackwell, Special Issue on Field and Service Robotics, 25 (6-7), pp.360-377, 2008.

[7] Foresti G.L. , Gentili S. and Zampato M., A vision-based system for autonomous underwater vehicle navigation, OCEANS '98 Conference Proceedings (Volume:1), pp 195-199, 1998.

[8] Krupinski S. , Allibert G. and Hamel T., Pipeline tracking for fully-actuated autonomous underwater vehicle using visual servo control, American Control Conference (ACC), pp 6196-6202, 2012.

[9] Jin-Yeong Park, Bong-Huan Jun, Pan-Mook Lee, Fill-Youb Lee and Jun-ho Oh, Experiment on Underwater Docking of an Autonomous Underwater Vehicle ISimI using Optical Terminal Guidance, OCEANS 2007, Europe, pp 1-6, 2007.

[10] J.-Y. Park, B.-H. Jun, P.-M. Lee and J. Oh, Experiments on vision guided docking of an autonomous underwater vehicle using one camera, Ocean Eng., Vol. 36, No. 1, pp. 48-61, Jan. 2009.

[11] Ura, T., Kurimoto, Y., Kondo, H., Nose, Y., Sakamaki, T. and Kuroda, (a) Searching Object Step (b) Visual Servoing Step (c) Docking Step (d) Docking Completed Successfully Fig. 15. Docking Process: (a) Searching Object Step, (b) Visual Servoing Step, (c) Docking Step, (d) Docking Completed Successfully Y., Observation behavior of an AUV for ship wreck investigation, Pro- ceedings of the OCEANS 2005 MTS/IEEE Conference, Vol.3, pp.2686- 2691, 2005.

[12] Palomeras, N., Ridao, P., Ribas, D. and Vallicrosa, G. Autonomous I-AUV docking for fixed-base manipulation, Preprints of the International Federation of Automatic Control, pp.12160-12165, 2014.

[13] Myo Myint, Kenta Yonemori, Akira Yanou, Mamoru Minami and Shintaro Ishiyama, Visual-servo-based Autonomous Docking System for Underwater Vehicle Using Dual-eyes Camera 3D-Pose Tracking, Proceedings of the 2015 IEEE/SICE International Symposium on System Integration, Nagoya, Japan, pp.989-994, 2015.

[14] Myo Myint, Kenta YONEMORI, Akira YANOU, Shintaro ISHIYAMA and Mamoru MINAMI, Robustness of Visual-Servo against Air Bubble Disturbance of Underwater Vehicle System Using Three-Dimensional Marker and Dual-Eye Cameras, Proceedings of the International Conference OCEANS15 MTS/IEEE, Washington DC, USA, pp.1-8, 2015.

[15] Lwin, KN.,Myint, M.,Mukada, N.,Yamada, D.,Minami, M.,Matsuno., T., Robustness of 3D pose Estimation against Turbidity Using Dual-eye Cameras And Active/Lighting 3D Marker for Visual-servoing Based AUV, OCEANS 宴 18 MTS/IEEE Kobe

[16] Lwin, KN.,Mukada, N.,Myint, M.,Yamada, D.,Minami, M., Matsuno., Docking Performance Against Turbidity Using Active Marker Under Day and Night Environment, AROB 23rd (2018)

[17] Maki, T., Shiroku, R., Sato, Y., Matsuda, T., Sakamaki, T. and Ura, T., Docking method for hovering type AUVs by acoustic and visual positioning, In Underwater Technology Symposium (UT), 2013 IEEE International (pp. 1-6), 2013.

[18] Suzuki. H and Minami. M, Visual Servoing to Catch Fish Using Global/Local GA Search, IEEE/ASME Transactions on Mechatronics, Vol.10, Issue 3, pp 352-357, 2005.

[19] Yu F., Minami M., Song W., Zhu J. and Yanou A., On-line head pose estimation with binocular hand-eye robot based on evolutionary model-based matching, Journal of Computer and Information Technology, Vol.2, No.1, pp.43-54, 2012.

[20] Song W. and Minami M., 3-D Visual Servoing Using Feedforward Evolutionary Recognition, Journal of the Robot Society of Japan, Vol.28, No.5, pp.591-598 (in Japanese), 2010.

[21] Wei. Song, M. Minami, Fujia Yu, Yanan Zhang and Akira Yanou, 3-D Hand and Eye-Vergence Approaching Visual Servoing with Lyapunouv-Stable Pose Tracking, IEEE Int. Conf. on Robotics and Automation (ICRA), pp. 5210-5217, 2011.

[22] W. Song, M. Minami and S. Aoyagi, On-line Stable Evolution- ary Recognition Based on Unit Quaternion Representation by Motion-Feedforward Compensation, International Journal of Intelligent Computing in Medical Sciences and Image Processing (IC-MED) Vol. 2, No. 2, pp.127-139 ,2007.

[23] Yu Cui, Kenta Nishimura, Yusuke Sunami, Mamoru Minami, Takayuki Matsuno and Akira Yanou, Analyses about Trackability of Hand-eye-vergence Visual Servoing in Lateral Direction, OPTIROB Conference, Romania, 2015.

[24] Song W, Minami M, Aoyagi S, On-line stable evolutionary recognition based on unit quaternion representation by motion-feedforward compensation, International Journal of Intelligent Computing in Medical Sciences & Image Processing, 2(2), pp.127-139, 2008.